Glass Struct. Eng. (2020) 5:67–82
https://doi.org/10.1007/s40940-019-00103-8

SI: GLASS PERFORMANCE PAPER

Pseudo-elastic cavitation model—part II: extension to cyclic behavior of transparent silicone adhesives

M. Drass · N. Bartels · J. Schneider · D. Klein

Received: 17 March 2019 / Accepted: 7 August 2019 / Published online: 27 August 2019

Abstract This study investigates the cyclic structural behaviour of adhesive joints of glass and metal using thin, structural silicone adhesives in heavily constrained applications. Based on cyclic uniaxial tensile tests on dog-bone and pancake test samples, the pseudo-elastic cavitation model from part I of this publication will be extended to describe two phenomenons: stress softening due to Mullins effect, as well as a mechanical hysteresis occurring under hydrostatic loading of rubber-like materials. This mechanical hysteresis under hydrostatic loading is associated with the growth and shrinkage of microscopic voids in the materials structure, and shows distinctive differences to the mechanical hysteresis known from isochoric test samples. In order to transfer the already presented pseudo-elastic cavitation model to describe the cyclic material behaviour, the isochoric part of the cavitation model is extended according to the classical theory of pseudo-elasticity to numerically describe stress softening under isochoric deformations. In addition, the volumetric part is provided with a special material formulation so that it can numerically reproduce the void growth hysteresis under cyclic volumetric tests, e.g. pancake tests. For validation, three-dimensional simulations of both cyclic tensile tests (dog-bone and pancake tests) are carried out.

M. Drass (✉) · N. Bartels · J. Schneider · D. Klein
Institute of Structural Mechanics and Design, Technische Universität Darmstadt, Franziska-Braun-Str. 3, 64287 Darmstadt, Germany
e-mail: drass@ismd.tu-darmstadt.de

Keywords Cavitation · Mullins effect · Void growth hysteresis · Cyclic pancake tests · Extended pseudo-elastic cavitation model · Hydrostatic loading of rubber

Abbreviations

EPDM	Ethylene-propylene-diene-monomer
PP	Polypropylene
NR	Natural rubber
PDMS	Polydimethylsiloxane
PC	Pancake test
DIC	Digital image correlation

List of symbols

$\Psi(\bullet)$	Helmholtz free energy
$\mathbf{F}$	Deformation gradient
$\mathbf{b}$	Left Cauchy–Green tensor
$\bar{\mathbf{b}}$	Isochoric left Cauchy–Green tensor
J	Relative volume
$\mathbf{I}$	Second order identity tensor
$\mathcal{I}$	Fourth order identity tensor
$\boldsymbol{\sigma}$	Cauchy stress tensor
p	Hydrostatic stress
Ω	Shape function
$\mathcal{D}_{\text{cav}}$	Dissipated energy due to void growth
η_{iso}	Isochoric Mullins variable
$\hat{\Psi}_{\text{iso,max}}$	Isochoric history variable
r	Isochoric Mullins material parameter

m	Isochoric Mullins material parameter
erf (x)	Error function
$\mathbb{D}_{\text{iso}}$	Driving force isochoric Mullins effect
ς	Volumetric softening/healing variable
η_{vol}	Volumetric softening variable
r_{vol}	Volumetric softening material parameter
m_{vol}	Volumetric softening material parameter
$\mathbb{D}_{\text{vol}}$	Driving force volumetric Mullins effect
η_{heal}	Volumetric healing variable
r_{heal}	Volumetric healing material parameter
m_{heal}	Volumetric healing material parameter
$\mathbb{D}_{\text{heal}}$	Driving force volumetric healing effect

1 Introduction

1.1 Motivation

With regard to the experimental investigations and results of the analysed transparent structural silicone adhesive TSSA according to "Appendices A and B", in which cyclic uniaxial tensile tests and cyclic pancake tests were investigated, a very interesting and so far unknown structural behaviour could be observed.

With respect to the structural behavior of the thin silicone adhesive TSSA produced by Dow Chemical Company, the material behaves according to the properties of the Mullins effect when analysing so-called dog bone samples under uniaxial cyclic loading. A typical and pronounced stress softening can be clearly seen on the unloading path (see Fig. 1a). Looking at the reloading path, the material shows the same structural response according to the unloading path until the previously reached maximum value of deformation is exceeded. Then the material response corresponds to the response of a virgin material. Furthermore, it is important to note that no healing or recovery effects under cyclic uniaxial loading could be observed. Therefore, the stiffness of the unloading and reloading paths is identical for large areas of applied deformation. This behaviour is well-known for isochoric deformations of rubber-like materials.

In the majority of the experimental investigations and industrial usage of rubber-like materials, the material behaves almost isochoric (foams excepted). Only under heavily constrained conditions, like in thin adhesive silicone layers used in the connection of glass façades, the material can no longer be treated as isochoric, and the volumetric properties have to be investigated carefully. Regarding the cyclic pancake test according to "Appendix B", the materials response under hydrostatic loading may be investigated. The mechanical hysteresis occurring at cyclic pancake test shows remarkable differences to the mechanical hysteresis occurring under isochoric loading conditions. In the unloading path, the material shows softening as it is known from isochoric test samples. However, the reloading path does not follow the unloading path which one would expect according to the theory of the classical Mullins effect (see Fig. 1b). In general, the Mullins effect is irreversible for some materials, but it can recover at high temperatures, which takes time. Looking at Fig. 1b, the material seems to recover instantly under cyclic hydrostatic loading. This implies that the effect is not associated with the classical Mullins effect, but takes place as elastic void growth and shrinkage which may be observed under hydrostatic loading. However, since in the reloading path a slightly reduction of the maximum reached stress level is observed, a combination of void growth hysteresis through elastic pore growth and shrinkage and real iso-

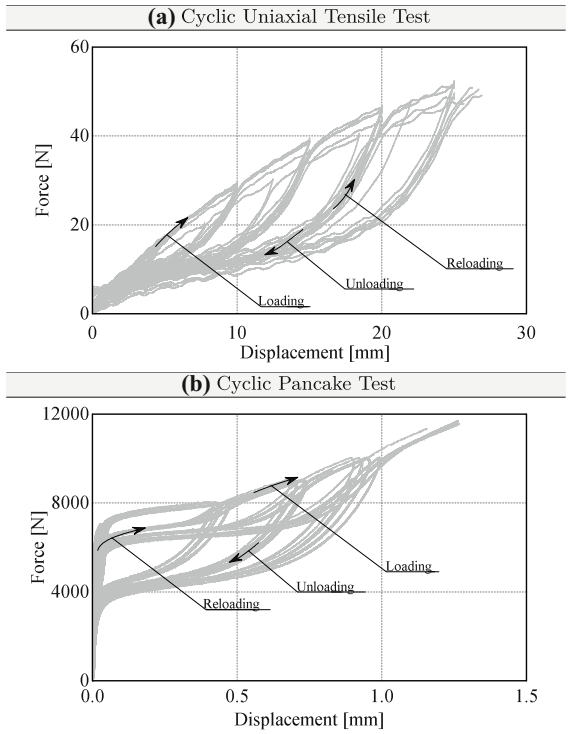

Fig. 1 Exemplary structural behaviour of TSSA under **a** uniaxial and **b** constrained cyclic loading (Pancake Test) with schematic representation of the loading, unloading and reloading paths

choric Mullins damage through possible bond breakage and filler rupture must be present.

Therefore, referring to part I of the present investigations (Drass et al. 2019), a modified pseudo-elastic approach must be formulated for the volumetric part of a general Helmholtz free energy function based on Ogden and Roxburgh (1999), which can represent void growth hysteresis phenomenologically according to the present cyclic loading condition.

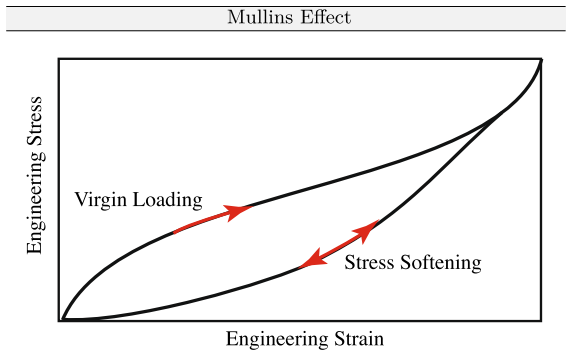

Fig. 2 Schematic Mullins effect

1.2 Some features of the Mullins effect

Loading filled elastomers cyclically, Bouasse and Carrière (1903) already discovered a distinct difference in the stress-strain behavior between virgin, unloading and reloading path in the experiments carried out, which manifests itself with a distinct **softening effect** in the structural response of the elastomers. This phenomenon was further investigated by Mullins (1949) and Mullins and Tobin (1965), whereby this effect was designated as Mullins effect. In their studies, the softening effect for unfilled and filled elastomers was experimentally investigated. It was found that in both types of elastomers a softening in the structural response could be detected during the unloading. A schematic representation of the Mullins effect is shown in Fig. 2.

Under some conditions, the material may experience **healing** or **recovery**, where—after thermal treatment of the material—the stiffness on the reloading path may be greater than in comparison to the unloading path, i.e. the material has experienced healing (DAmbrosio et al. 2008). A second definition of healing or recovery of elastomers exposed to cyclic loading is described when the residual strains or the permanent set can be reduced by temperature storage or by the removal of specimens with long relaxation times, so that the residual strains almost drop to zero. The test sample is then not exposed to external loads during the relaxation time or temperature storage, so that it can deform free of constraint. Different experiments to describe the healing effect in rubbers were carried out, for example, by Mullins (1948), who investigated stress-recovery of a filled NR under temperature influence and sample storage for a certain period of time. He found that with increasing temperature or storage time the healing effect in the form of reduction of residual strains in the material increased significantly. In contrast, for a carbon black filled NR only a small amount of healing was observed even during a relaxation period of 4 weeks (Mullins 1948). During the studies on healing of Hanson et al. (2005) on a silica-filled PDMS, it was found that even at the relaxation period of 6 months no recovery took place, so it is not surprising that Diani et al. (2009) state that this effect can be neglected with standard application in indoor climate. In contrast to these investigations, the cyclic pancake tests seem to show significant recovery without being exposed to heat for a longer time. This implies that the origin of the mechanical hysteresis is not due to the microscopic effects associated with Mullins, but rather with the growth and shrinkage of voids under hydrostatic loading.

A unified theory for the physical interpretation of the Mullins effect does not yet exist. Therefore, three descriptive models for the characterization of the Mullins effect are briefly discussed below. In the early investigations of Blanchard and Parkinson (1952), it is assumed that stress softening occurs as a result of the Mullins effect by so-called bond rupture between polymer chain and filler. This idea was taken up by Bueche (1960) and further explained by the fact that the physical bond between polymer and filler is weaker than the chemical bond between the Kuhn segments of the polymer chain. When the polymer chain between two filler particles is completely stretched, fracture must take place at the filler–matrix-interaction according to that model, since on the one hand the weaker bond is present and on the other hand it is assumed that the Kuhn segments are rigid and therefore cannot be further stretched. Another theory on the Mullins effect states that during the initial loading molecules slip over the surface of the fillers and new bonds are formed along the chains (Houwink 1956). The model conception of molecules slipping is equivalent to the change

of entropy in the material, which may be restored to the almost original dimension by temperature input, which corresponds to the experimental results of Mullins (1948). The third model assumes a rupture of the filler agglomerates or aggregates, since in the experimental investigations of Kraus et al. (1966) neither the theory of bond rupture, molecule slipping nor the formation of vacuoles at the matrix–filler-interaction were sufficient to explain the observed Mullins effect.

1.3 Methodology

In this paper an extension of the previously presented pseudo-elastic cavitation model (Drass et al. 2019) is introduced in order to describe the structural behaviour of silicone adhesives under cyclic loading. The basic idea is to transfer the classical description of pseudo-elasticity for stress softening under cyclic loading according to Ogden and Roxburgh (1999) to the pseudo-elastic cavitation model presented in part I of the present study (Drass et al. 2019). The advantages of the approach of pseudo-elasticity lie in the simple formulation, where the strain energy function can be completely described at a macro-scale, the application of the volumetric-isochoric split, which brings advantages regarding the material parameter identification and the avoidance of computationally intensive and complex multi-scale modelling methods.

2 General concept

Since the pseudo-elastic approach of Lazopoulos and Ogden (1998) has already been presented in part I (Drass et al. 2019), only the essential equations necessary for deriving the extended pseudo-elastic cavitation model for cyclic loading are summarized below.

Assuming a general Helmholtz free energy function $\Psi(\mathbf{F})$ that depends solely on the deformation gradient $\mathbf{F}$, the pseudo-elastic approach to this problem reads

$$\Psi(\mathbf{F}, \eta) = \eta\, \hat{\Psi}(\mathbf{F}) + \phi(\eta), \tag{1}$$

which is capable of describing the classical Mullins effect in rubbers and rubber-like materials phenomenologically. In this context, $\phi(\eta)$ describes a damage function, which serves to determine the damage parameter $\eta \in [0, 1]$ implicitly in terms of the state of deformation through an additionally proposed equilibrium equation

$$\frac{\partial \Psi(\mathbf{F}, \eta)}{\partial \eta} = 0. \tag{2}$$

This general concept is now specifically applied to separately describe the effects proposed in Sect. 1.1 with respect to isochoric and volumetric deformations.

3 Extended pseudo-elastic cavitation model

3.1 Isochoric Mullins damage under cyclic loading

To describe the isochoric Mullins effect phenomenologically with the pseudo-elastic approach, exactly the model proposed by Ogden and Roxburgh (1999) is used, in which the isochoric part of any Helmholtz free energy function becomes

$$\Psi_{\mathrm{iso}}\left(\bar{\mathbf{b}}, \eta\right) = \eta_{\mathrm{iso}}\, \hat{\Psi}_{\mathrm{iso}}\left(\bar{\mathbf{b}}\right) + \phi\left(\eta_{\mathrm{iso}}\right). \tag{3}$$

Since the isochoric–volumetric split accordingly to Flory (1961) was applied, the isochoric Helmholtz free energy function is only dependent on the isochoric left Cauchy–Green tensor $\bar{\mathbf{b}}$.

By satisfying the additional equilibrium equation of Eq. (2) arising from the inclusion of an internal variable in the constitutive model, the damage variable η_{iso} reads

$$\eta_{\mathrm{iso}} = 1 - \frac{1}{r}\mathrm{erf}\left[\frac{\left(\hat{\Psi}_{\mathrm{iso,max}}\left(\bar{\mathbf{b}}\right) - \hat{\Psi}_{\mathrm{iso}}\left(\bar{\mathbf{b}}\right)\right)}{m}\right]. \tag{4}$$

In this context, $r \in]1, \infty]$ and $m \in]0, \infty]$ are material parameters, which must be determined through experiments. The operator erf $(\bullet)$ describes the error function, which is a sigmoid function. It is often used in statistics and in the theory of partial differential equations and is closely related to the error integral. It is generally defined by

$$\mathrm{erf}(x) = \frac{2}{\sqrt{\pi}} \int_0^x e^{-t^2} dt. \tag{5}$$

For a positive argument x, the error function has the value range of erf $(x) \in [0, 1]$.

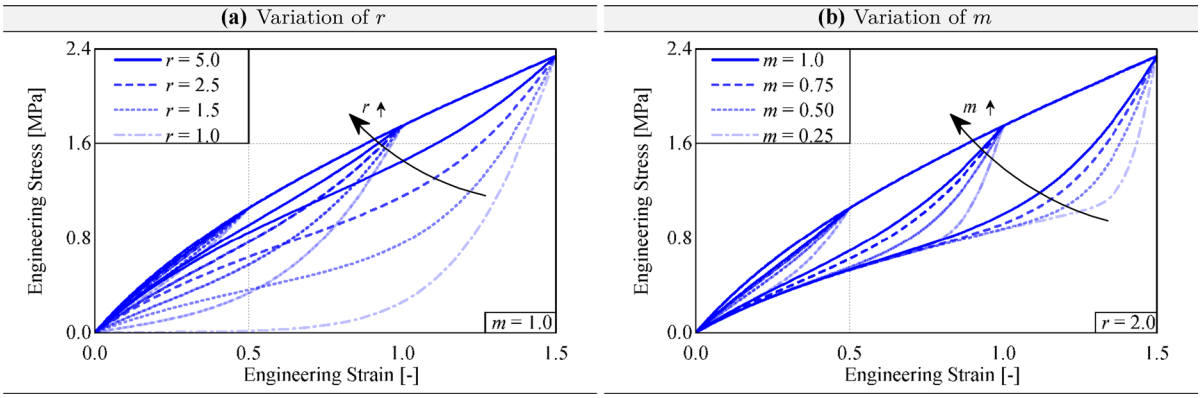

Fig. 3 Exemplary structural behavior of one-element test under cyclic uniaxial tensile loading varying the parameter **a** r with $m = 1.0$ and **b** m with $r = 2.0$

Returning to the governing parameters of η_{iso}, the larger r is chosen, the less the influence of Mullins effect on the structural response of the material under cyclic loading. In contrast, parameter m describes in particular how much softening occurs in the case of small deformations. The smaller m is chosen, the more softening occurs at small deformations. The strain energy $\hat{\Psi}_{\text{iso,max}}$ is a history variable and stores the maximum reached isochoric strain energy density during loading history. To better illustrate the influence of parameters m and r, the structural responses are shown separately in Fig. 3 for each varying parameter for a uniaxial one-element test under cyclic loading. A normalized, incompressible Neo-Hooke material model with $\mu = 1.0$ MPa was coupled with the pseudo-elastic approach according to Ogden and Roxburgh (1999).

Due to the choice of the pseudo-elasticity approach, the calculation of the isochoric Cauchy stress tensor simplifies significantly, as all partial derivatives of the isochoric Helmholtz free energy function with respect to the damage variable disappear. Hence, the isochoric Cauchy stress tensor reads

$$\boldsymbol{\sigma}_{\text{iso}} = \eta_{\text{iso}} \left[\mathcal{I} - \frac{1}{3}\mathbf{I} \otimes \mathbf{I} \right] : \frac{\partial \hat{\Psi}_{\text{iso}}}{\partial \bar{\mathbf{b}}} \left(\bar{\mathbf{b}} \right), \tag{6}$$

where $\mathbf{I} \otimes \mathbf{I}$ represents the dyadic product of two second order identity tensors and $\mathcal{I}$ describes a fourth-order identity tensor. It can be clearly seen from Eq. (6), if η_{iso} is inactive ($\eta_{\text{iso}} = 1$), then the classic undamaged material response is obtained, whereas stress softening only occurs when η_{iso} is active ($\eta_{\text{iso}} < 1$). This means η_{iso} is only active if $\hat{\Psi}_{\text{iso,max}} \left(\bar{\mathbf{b}} \right) \neq \hat{\Psi}_{\text{iso}} \left(\bar{\mathbf{b}} \right)$, which is generally the case for unloading and for reloading until the previously maximum reached strain energy is exceeded. Then, $\hat{\Psi}_{\text{iso}} \left(\bar{\mathbf{b}} \right)$ and $\hat{\Psi}_{\text{iso,max}} \left(\bar{\mathbf{b}} \right)$ are identical again.

3.2 Volumetric softening and recovery under cyclic loading

In the following, an extension of the pseudo-elastic cavitation model proposed by Drass et al. (2019) is presented, which is intended to describe the structural behavior of the pancake test under cyclic loading phenomenologically. As previously mentioned, individual sections of the structural response of TSSA under constrained cyclic tension could be assigned to different phenomena (see "Appendix B"). Starting with an elastic pore growth during virgin loading, it is followed by an irreversible void growth hysteresis for unloading and a dominant instantaneous healing for reloading.

The primary or virgin loading path shows stress softening due to the cavitation effect (Drass et al. 2018a) and can be represented with the pseudo-elastic cavitation model presented in part I of the present studies, which reads in a general form

$$\Psi = \Psi_{\text{iso}} \left(\bar{\mathbf{b}} \right) + \Psi_{\text{vol,ND}} \left(J \right) + \Omega \, \mathcal{D}_{\text{cav}} \left(J \right) + \phi \left(\Omega \right). \tag{7}$$

For reasons of clarity for the subsequent model extension, all operational terms of the pseudo-elastic cavitation model representing stress softening due to void growth are grouped together as

$$\Psi_{\text{cav}} = \Psi_{\text{vol,ND}}\left(J\right) + \Omega\ \mathcal{D}_{\text{cav}}\left(J\right) + \phi\left(\Omega\right), \tag{8}$$

so that the pseudo-elastic Helmholtz free energy function is now briefly described by

$$\Psi = \Psi_{\text{iso}} + \Psi_{\text{cav}}. \tag{9}$$

Further, looking at the cyclic pancake tests presented in Fig. 1b, the unloading paths showed an additional material softening, where all experimental curves meet at a force level of 3.600 kN and then decrease to zero again with full unloading. A suitable approach to represent this phenomenon is the application of the classical pseudo-elastic approach according to Ogden and Roxburgh (1999) to Ψ_{cav} in order to characterize softening under cyclic loading. As mentioned before, the instant recovery of the volumetric softening indicates other effects than the classical Mullins effect, which is associated with microscopic reformation mechanisms of both polymer chains and filler particles. The volumetric softening, which instantly recovers, seems to be associated with the growth and shrinkage of microscopic voids in the material. Nonetheless, the softening can be modeled with a pseudo-elastic approach in analogy to the Mullins effect. Since the classical approach of Ogden and Roxburgh (1999) to describe the Mullins effect is not able to represent healing or recovery effects, it needs to be extended with respect to a healing variable. This is necessary because from the cyclic pancake tests a kind of recovery effect could be observed for all reloading paths up to a force level of approximately 6000 kN (see "Appendix B"). Here, it could be shown experimentally that the unloading and reloading paths differ significantly, so that it is obvious to introduce an additional variable to describe the recovery effect.

To take into account the effects of softening on the unloading and healing on the reloading path phenomenologically, Eq. (9) is now extended through the already presented pseudo-elastic approach, which leads to

$$\Psi = \Psi_{\text{iso}} + \varsigma\ \Psi_{\text{cav}} + \phi\left(\varsigma\right). \tag{10}$$

In this context, $\phi\left(\varsigma\right)$ represents a damage or healing function depending on the current loading condition and ς characterizes a history variable that determines the amount of volumetric softening for unloading and the amount of healing for the reloading conditions.

For the present approach, the Cauchy stress tensor with respect to Ψ_{cav} is calculated exactly in line with Sect. 3.1, which leads to

$$\begin{aligned}\boldsymbol{\sigma}_{\text{cav}} &= \frac{2}{J}\left[\frac{\partial \Psi_{\text{cav}}}{\partial \mathbf{b}}\left(J,\varsigma\right) + \underbrace{\frac{\partial \Psi_{\text{cav}}}{\partial \varsigma}\left(J,\varsigma\right)}_{=0}\frac{\partial \varsigma}{\partial \mathbf{b}}\left(\mathbf{b}\right)\right]\mathbf{b} \\ &= \frac{\partial \Psi_{\text{cav}}}{\partial J}\left(J,\varsigma\right)\ \mathbf{I}.\end{aligned} \tag{11}$$

Here, too, the calculation of the stress tensor $\boldsymbol{\sigma}_{\text{cav}}$ could be considerably simplified due to the additional equilibrium condition

$$\frac{\partial \Psi_{\text{cav}}}{\partial \varsigma}\left(J,\varsigma\right) = 0, \tag{12}$$

which results from the inclusion of the additional internal variable ς in the pseudo-elastic constitutive model.

In order to describe the phenomenological constitutive model completely, the internal damage variable ς must be defined more precisely. Starting with the description of the volumetric Mullins damage, a slightly modified approach according to Ogden and Roxburgh (1999) is used, which reads

$$\bar{\varsigma} = 1 - \underbrace{r_{\text{vol}}\ \text{erf}\left(\frac{\Psi_{\text{cav,max}} - \Psi_{\text{cav}}}{m_{\text{vol}}}\right)}_{=\eta_{\text{vol}}}. \tag{13}$$

Since Eq. (13) does not represent the final form for the internal damage variable representing volumetric softening and possible healing effects, ς is provided with an bar. For the sake of clarity, the variable for volumetric softening is designated η_{vol}, which depends on two material parameters, $r_{\text{vol}} \in [0, 1]$ and $m_{\text{vol}} \in\ ]0, 1]$, and the difference between the maximum reached (volumetric) strain energy $\Psi_{\text{cav,max}}$ and the current strain energy Ψ_{cav}. This is a standard approach that has been used to describe the isochoric Mullins effect in particular (Zhang et al. 2011), but has been transferred here in order to investigate softening due to volumetric deformations.

In order to transfer the standard approach of Eq. (13) to possible healing effects, Bartels (2018) proposed an ansatz in which η_{vol} is again multiplied by an additional healing variable η_{heal}, which is also

defined in the same manner as η_{vol}. The healing variable reads

$$\eta_{\mathrm{heal}} = r_{\mathrm{heal}}\ \mathrm{erf}\left(\frac{\bar{\varsigma} - \bar{\varsigma}_{\mathrm{min}}}{m_{\mathrm{heal}}}\right), \qquad \bar{\varsigma}_{\mathrm{min}}(\mathrm{t}) = \min\left[\bar{\varsigma}(\tau),\ \tau \leq \mathrm{t}\right] \tag{14}$$

where $r_{\mathrm{heal}} \in [0, 1]$ and $m_{\mathrm{heal}} \in\ ]0, 1]$ are material parameters describing the course of healing. Since according to the results of the pancake tests the healing variable can only be active ($\eta_{\mathrm{heal}} > 0$) on the reloading path, its driving force is the difference between the current and the minimum volumetric Mullins damage. When the reloading path exceeds the previously occurred maximum, the stress follows the virgin curve, on which no healing should occur. To uniquely characterize the reloading path, and to differentiate it from the virgin curve, the healing variable has to be reset as soon as the previously occurred maximum deformation is exceeded. From a thermodynamical point of view, this reset of the healing variable has to be seen critical. Nevertheless, no further thermodynamic investigations are carried out in this work, so that the model is purely phenomenological. In summary, the internal damage variable is completely defined by

$$\varsigma = 1 - \eta_{\mathrm{vol}}\,(1 - \eta_{\mathrm{heal}})\,, \tag{15}$$

with $\varsigma \in [0, 1]$. Assuming no healing occurs in the material, i.e. $\eta_{\mathrm{heal}} = 0$, the classic approach for volumetric Mullins damage is present, where the unloading and reloading path are identical. Upon complete healing of the material, the reloading path is equal to the virgin material response, but the structural response for the unloading path exhibits stress softening caused by the void growth and shrinkage.

In order to gain a better understanding of the presented material model, which can represent cavitation, isochoric Mullins effect and volumetric softening and healing due to reversible pore growth, the load history of a one-element test under cyclic hydrostatic loading is examined below as an example. Looking at Fig. 4a, the load history of a cyclic hydrostatic tensile test is shown separately for virgin loading, unloading and reloading. Additionally, the history variable ς is shown, which is a combination of the volumetric damage variable η_{vol} according to the unloading pathway and the healing variable η_{heal} for the reloading path according to Eq. (15). Figure 4b, c additionally show the development of the corresponding damage or healing variables. First, considering only the volumetric softening, Fig. 4b shows that softening only occurs when $\Psi_{\mathrm{cav,max}}$ is not equal to Ψ_{cav}. This is generally the case whenever one is on the unloading or reloading path. Consequently, the softening variable η_{vol} must assume values greater than zero, as shown in Fig. 4b. It should also be noted that the chosen driving force $(\Psi_{\mathrm{cav,max}} - \Psi_{\mathrm{cav}})$ to describe the volumetric softening effect exactly reflects the ranges of unloading and reloading, which justifies the chosen phenomenological approach. In contrast, looking at the course of the healing variable η_{heal}, Fig. 4c shows that, on the one hand, the selected driving force $(\bar{\varsigma} - \bar{\varsigma}_{\mathrm{min}})$ is a good measure to reproduce the recovery effect. On the other hand, the chosen formulation provides a clear distinction between virgin loading, unloading and reloading. Accordingly, healing occurs only on the reloading path until the maximum deformation reached before is exceeded. For the sake of completeness, the algorithmic box for the numerical treatment of the extended pseudo-elastic cavitation model for cyclic loading is given in Table 1.

3.3 Parameter studies on cyclic pseudo-elastic cavitation model

Since the existing material model is now dependent on parameters describing a volumetric softening and/or healing effect, a parameter study will be carried out in the following with regard to these parameters for reasons of comprehensibility. First, the influence of the parameter r_{vol} on the structural response under cyclic hydrostatic loading is investigated. For reasons of clarity, all healing effects have been excluded, so that $r_{\mathrm{heal}} = 0$. Figure 5a shows that this parameter determines the degree of softening compared to the virgin loading path.

It is notable that with an increasing r_{vol} the amount of softening increases also for the unloading path. Since no healing effects have been considered in the present study, the unloading and reloading paths are identical. Returning to the parameter r_{vol}, it gives the ratio between bifurcation load of the unloading paths and virgin loading path. Hence, it can be stated that

$$r_{\mathrm{vol}} \approx 1 - \frac{p_{\mathrm{cr}}^{\mathrm{vol}}}{p_{\mathrm{cr}}} \tag{16}$$

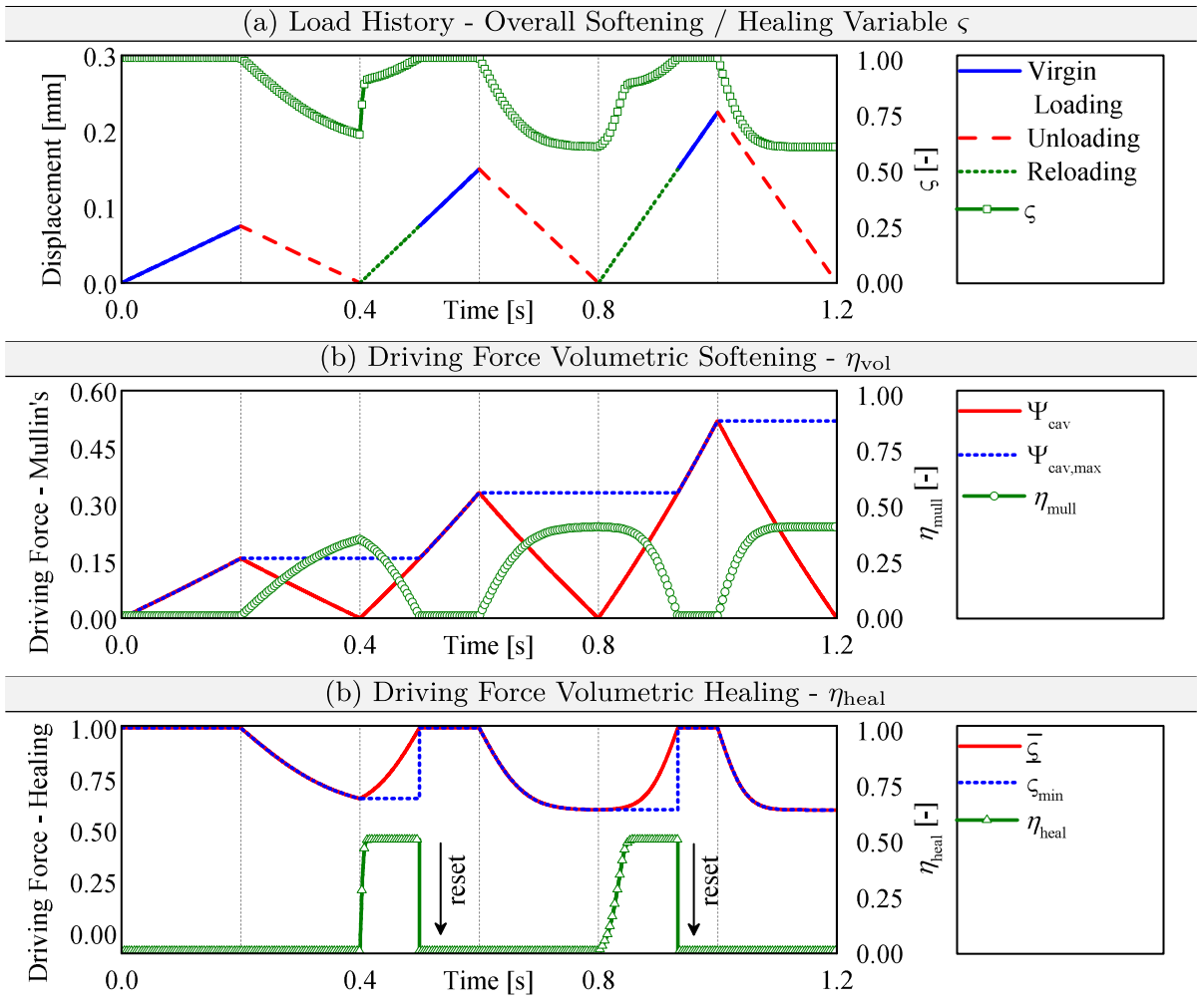

Fig. 4 Exemplary load history of cyclic hydrostatic tension loading

applies. In this context, p_{cr} describes the bifurcation point for the virgin load path, whereas $p_{\mathrm{cr}}^{\mathrm{vol}}$ characterizes the critical stress, at which all unloading and reloading curves coincide disregarding healing effects. Therefore, using Eq. (16), the material parameter r_{vol} for the volumetric softening can be calculated approximately directly from the experimental data obtained, for example, from the pancake tests.

A similar statement applies considering the bifurcation load of the reloading path when healing effects are present (see Fig. 5b). Here, the parameter r_{heal} can be described as the ratio of

$$r_{\mathrm{heal}} \approx \frac{p_{\mathrm{cr}}^{\mathrm{heal}} - p_{\mathrm{cr}}^{\mathrm{vol}}}{p_{\mathrm{cr}} - p_{\mathrm{cr}}^{\mathrm{vol}}}. \tag{17}$$

Considering the experimental results of the cyclic pancake test, in which all unloading and reloading curves converge to a specific load level, the knowledge of these approximate solutions for the parameters r_{vol} and r_{heal} is very valuable, since both material parameters can be approximated directly from the experimental results. It should also be mentioned that these approximation formulas also apply to inhomogeneous stress and strain states, as is the case with the pancake test, since these have just been developed from the experimental results of these tests.

If one also considers the parameter m_{vol} with neglect of healing, it is noticeable that it slightly influences $p_{\mathrm{cr}}^{\mathrm{vol}}$ on the one hand, and in particular controls the course of the softening at small to moderate deformations on

Table 1 An algorithmic box of the FE procedure

1. given: deformation gradient $\mathbf{F}$ at t_n and t_{n+1}
2. compute pseudo-elastic Helmholtz free energy function according to (Drass et al. 2019)
   $\Psi = \Psi_{\mathrm{iso}} + \Psi_{\mathrm{cav}}$
3. compute isochoric Mullins effect
   $\eta_{\mathrm{iso}} = 1 - \frac{1}{r}\,\mathrm{erf}\left[\frac{1}{m}\left(\Psi_{\mathrm{iso,max}} - \Psi_{\mathrm{iso}}\right)\right]$, where
   $\mathbb{D}_{\mathrm{iso}} = \Psi_{\mathrm{iso,max}} - \Psi_{\mathrm{iso}}$ represents the driving force for the isochoric Mullins effect
4. compute void growth hysteresis
   $\eta_{\mathrm{vol}} = r_{\mathrm{vol}}\,\mathrm{erf}\left(\frac{\Psi_{\mathrm{cav,max}} - \Psi_{\mathrm{cav}}}{m_{\mathrm{vol}}}\right)$, where
   $\mathbb{D}_{\mathrm{vol}} = \Psi_{\mathrm{cav,max}} - \Psi_{\mathrm{cav}}$ represents the driving force for the void growth hysteresis
5. compute recovery effect
   $\eta_{\mathrm{heal}} = r_{\mathrm{heal}}\,\mathrm{erf}\left(\frac{\bar{\varsigma} - \bar{\varsigma}_{\mathrm{min}}}{m_{\mathrm{heal}}}\right)$, where
   $\mathbb{D}_{\mathrm{heal}} = \bar{\varsigma} - \bar{\varsigma}_{\mathrm{min}}$ represents the driving force for the volumetric recovery effect
6. compute internal history variable ς accounting for void growth hysteresis
   $\varsigma = 1 - \eta_{\mathrm{vol}}\,(1 - \eta_{\mathrm{heal}})$
7. update (2) with internal history variable η_{iso} and ς to calculate Helmholtz free energy function and Cauchy stress tensor
   $\Psi = \underbrace{\eta_{\mathrm{iso}}\,\Psi_{\mathrm{iso}} + \phi\,(\eta_{\mathrm{iso}})}_{\text{isochoric Mullins Effect}} + \underbrace{\varsigma\,\Psi_{\mathrm{cav}} + \phi\,(\varsigma)}_{\text{volumetric softening and recovery}}$
   $\boldsymbol{\sigma} = \boldsymbol{\sigma}_{\mathrm{iso}} + \boldsymbol{\sigma}_{\mathrm{cav}} = \eta_{\mathrm{iso}}\,\boldsymbol{\sigma}_{\mathrm{iso},0} + \varsigma\,\boldsymbol{\sigma}_{\mathrm{cav},0}$

the other hand (see Fig. 5c). In addition, the structural behaviour dependent on the parameter m_{heal} is investigated taking into account healing. Figure 5d shows that with increasing m_{heal} one approaches the course of the unloading curve. In contrast, a very small m_{heal} causes a bifurcation point that lies between the virgin loading and the unloading path, as could be observed in the cyclic pancake tests. It should be noted here that the approximate solution of Eq. (17) is particularly true for a very small m_{heal}, whereas for a large m_{heal} the bifurcation point $p_{\mathrm{cr}}^{\mathrm{vol}}$ is approached.

Finally, the structural behavior of the cyclic pancake test will now be qualitatively represented by the pseudo-elastic cavitation model extended for cyclic loading. Therefore, a one-element test is analysed under cyclic hydrostatic tension, knowing that no pure hydrostatic stress state prevails in the pancake test (Drass et al. 2018b, c). Nevertheless, the adaptability of the phenomenological model should be presented within this study. The material parameters of the pure pseudo-elastic cavitation model were chosen according to Drass et al. (2018a), whereas the parameters describing volumetric softening and healing due to elastic pore growth and shrinkage were adaptively adjusted to qualitatively approximate the experimental results of the cyclic pancake test.

As the qualitative comparison in Fig. 6 shows, the extended pseudo-elastic cavitation model is well suited to reproduce material softening due to cavitation. Furthermore, the material softening caused by the void growth and shrinkage can also be approximated when the material is unloaded. Qualitatively, all unloading paths meet in one point ($p_{\mathrm{cr}}^{\mathrm{vol}}$) according to the experimental results. Finally, the healing effect due to elastic pore growth and shrinkage can also be simulated with the proposed model. It is further possible to reproduce the effect that all reloading curves coincide at one bifurcation point $p_{\mathrm{cr}}^{\mathrm{heal}}$ and then continue along the reloading path until the maximum previous deformation state is exceeded.

4 Numerical validation of the constitutive model

In this section, the numerical simulations of the cyclic uniaxial tensile tests and the cyclically loaded pancake tests are performed using three-dimensional full-

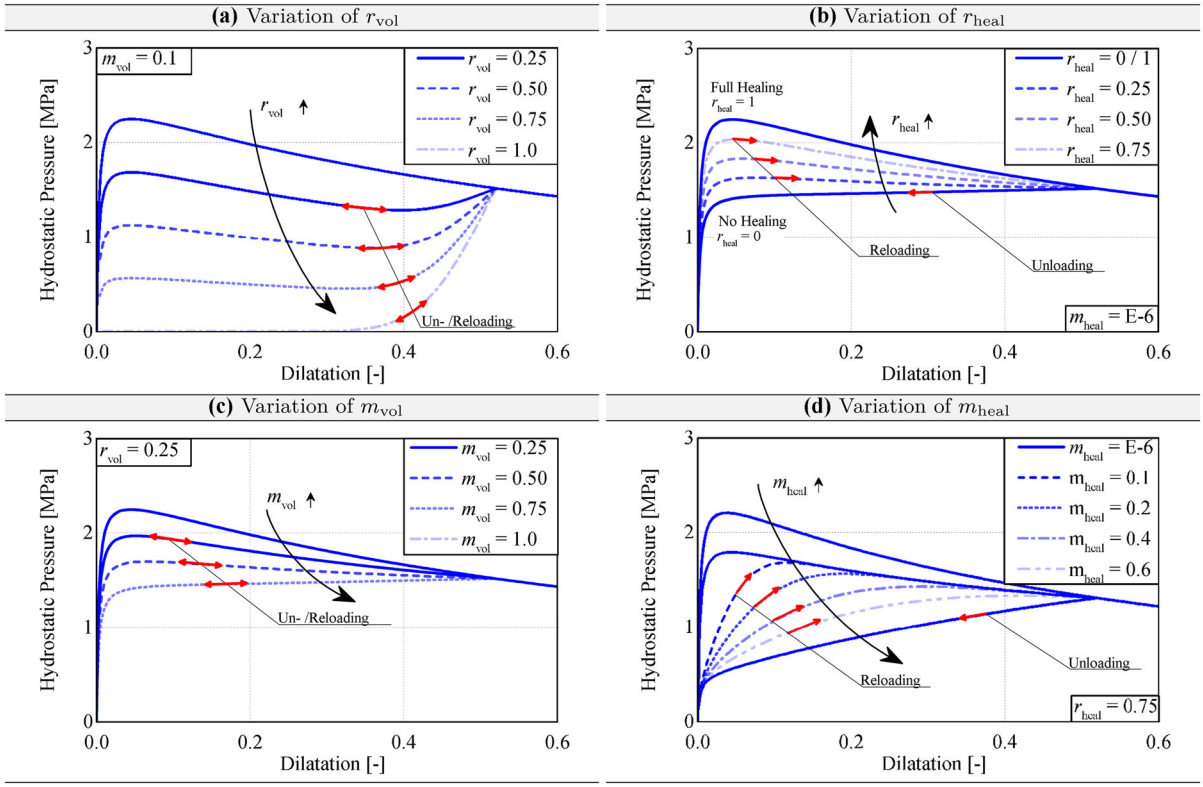

Fig. 5 Parameter studies on the extended pseudo-elastic cavitation model accounting for volumetric softening and healing respectively by variation of the parameters **a** r_{vol}, **b** r_{heal}, **c** m_{vol} and **d** m_{heal}, whereby all other parameters were set constant

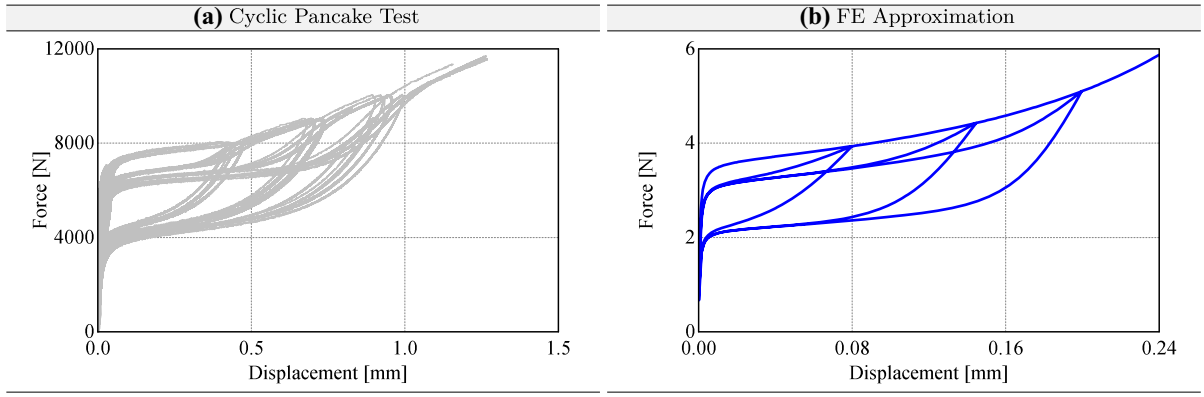

Fig. 6 Qualitative comparison between cyclic pancake test and numerical simulation of a one-element test under cyclic hydrostatic load using the extended pseudo-elastic cavitation model

scale finite element calculations. For this purpose, the extended pseudo-elastic cavitation model presented in Sect. 3 is implemented in ANSYS FE code, which is able to simulate the softening of isochoric deformations due to the Mullins effect. Furthermore, it is able to characterize the reversible softening due to void growth hysteresis under volumetric deformations.

The utilized material parameters of the extended pseudo-elastic cavitation model are summarized in Table 2 in "Appendix C". The material parameters for

the description of the cyclic behaviour were determined by inverse numerical methods. For a more detailed description of the inverse determination of material parameters, the authors refer to Drass et al. (2017). As already described in the presentation of the extended pseudo-elastic cavitation model in Sect. 3, the parameters r_{vol} and r_{heal} can be read directly from the experimental data of the cyclic pancake tests via Eqs. (16) and (17) respectively. All other parameters to describe the isochoric Mullins effect and the volumetric void growth hysteresis had to be calculated based on the above-mentioned inverse material parameter identification.

The numerical simulations of the cyclic tests were carried out based on three-dimensional volume models. In order to save computing time, corresponding boundary conditions were applied in the model in order to have to calculate only a section of the cyclically loaded samples. The displacement boundary conditions were programmed according to the experimental test routine used. The results of the simulation are shown in Fig. 7. Since the pseudo-elastic cavitation model from part I can now be enhanced by adding the effects of (i) isochoric Mullins/(ii) irreversible void growth hysteresis (iii) void growth hysteresis, three graphs are plotted to study the effect of successively adding these phenomena.

Starting with the numerical simulation of the cyclic tensile tests, an irreversible Mullins effect could be observed from the experiments, which can be reproduced with the isochoric pseudo-elastic approach of Ogden and Roxburgh (1999). As shown in Fig. 7a, the pronounced material softening can be reproduced on the unloading path. Furthermore, the effect of virgin stiffness on reaching and exceeding the previously achieved maximum deformation can be approximated very well. Looking at the simulation of the cyclic pancake test (see Fig. 7b), the isochoric Mullins effect

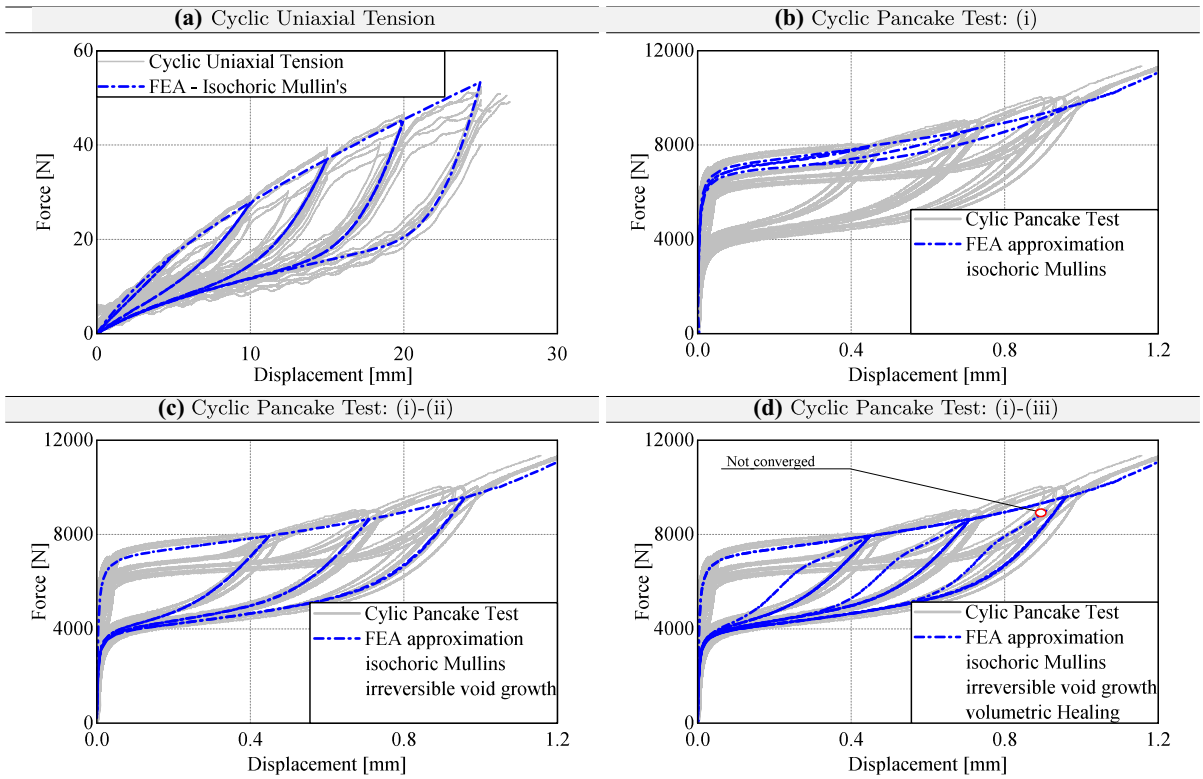

Fig. 7 Numerical validation of the cyclic tensile test under consideration of **a** isochoric Mullins effect. Numerical validation of cyclic pancake test under consideration of **b** isochoric Mullins effect, **c** Mullins and irreversible void growth hysteresis and **d** Mullins and void growth hysteresis

has only a small impact on the simulation result. This is also obvious, since in the pancake test a predominantly volumetric deformation takes place, whereas isochoric stresses and strains only occur at the edges. By adding the volumetric void growth hysteresis effect to the material model, it can be seen that the strongly pronounced material softening can be approximated during unloading (see Fig. 7c). However, it is not yet possible to numerically describe the healing effect. In the last simulation of the cyclic pancake test, the effects of isochoric and volumetric Mullins effect are coupled to the healing effect at reloading with the pseudo-elastic cavitation model. As can be seen in Fig. 7d, it is possible to represent the healing effect on the reloading paths. However, it should be noted that the experimental curves are not quite met, which is due to numerical problems. For large deformations within the reloading path, it can be clearly seen that the simulation and experiment fit well together. However, the bifurcation point is not encountered during reloading. For this, the parameter m_{heal} would have to be selected much smaller in order to recalculate the cyclic pancake tests. However, if the parameter $m_{\text{heal}} << 0.07$ is selected, there is no more convergence during the Newton-Raphson iterations, therefore further investigations are required. Nonetheless, the validation presented here and the parameter study from Sect. 3.3 have shown that the extended pseudo-elastic cavitation model is very well suited to represent the cavitation effect, isochoric Mullins effect and the void growth hysteresis including healing effects during reloading.

5 Conclusions

The aim of this paper was to extend the pseudo-elastic cavitation model presented in part I in order to numerically characterize the cyclic behavior (isochoric and volumetric) of a transparent structural silicone, here TSSA. The cyclic behaviour of TSSA was first briefly presented, with the exact experimental results being summarized in "Appendices A and B" for reasons of clarity. To describe the isochoric cyclic behaviour of TSSA numerically, the pseudo-elastic cavitation model, or only the isochoric part of it, was equipped with the Ogden and Roxburgh (1999) approach. This makes it possible to represent stress softening due to the Mullins effect very well. Since in cyclic pancake tests also softening—together with an instant recovery—occurs, the volumetric part of the pseudo-elastic cavitation model must additionally be extended with damage and healing variables. Consequently, the classical pseudo-elastic approach according to Ogden was applied to the volumetric part and extended with a healing variable. The healing is—up to this point—not thermodynamic consistent and only phenomenological motivated. Future investigations should aim for thermodynamic consistent formulations of the void growth hysteresis.

The one-element test showed that stress softening as well as healing can be approximated according to the structural behavior in the cyclic pancake test. To validate the extended pseudo-elastic cavitation model numerically, three-dimensional FE simulations of the cyclic tensile test and the cyclic pancake test were performed. The numerical recalculation of the cyclic tensile tests yielded very good results. Considering the simulation of the cyclic pancake tests, the cavitation effect as well as the softening on the unloading path could be represented very well. The numerical simulation of the healing led to numerical problems regarding the convergence. However, it should be noted that all effects could be described in an orderly way. Further research deals with the improvement of the numerical stability in order to be able to map the healing effects due to cyclic loading in three-dimensional calculations.

Furthermore, the cyclic behaviour of the transparent structural silicone has to be investigated under fatigue aspects. The aim here is to clarify how the material behaves in such a large number of hysteresis loops. The aim is to clarify whether Mullins effect and void growth hysteresis can be recognized as dominant even under fatigue loading.

Acknowledgements We would like to gratefully thank The Dow Chemical Company ("DOW") for their support during our studies. In addition, we would like to thank Glas Trösch Holding AG and in particular Bruno Kassnel-Henneberg for the production of all test specimens.

A Cyclic uniaxial tensile tests

Special cyclic uniaxial tensile tests were performed to experimentally characterize the cyclic behavior of TSSA and to observe the effect of stretch-induced whitening of the test sample. Therefore, midget tensile tests were carried out under the light microscope in order to assign high-resolution images of the sur-

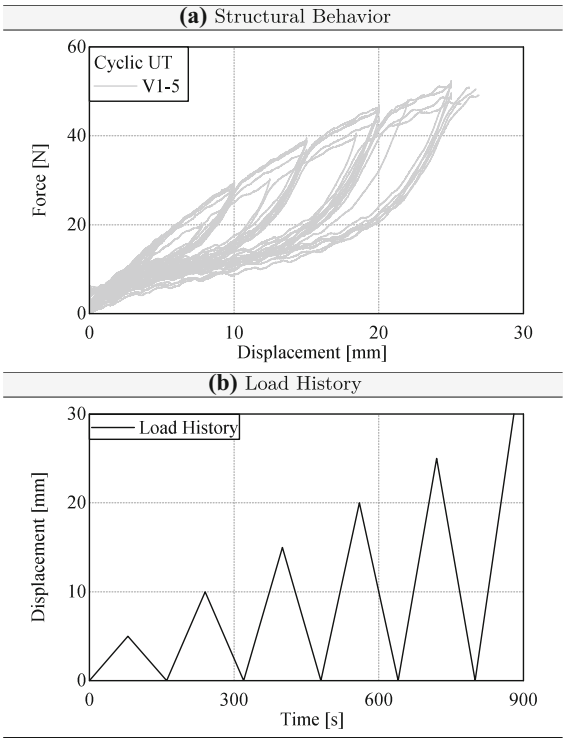

Fig. 8 Experimental test results for TSSA under cyclic uniaxial tensile loading: **a** force–displacement curves and **b** load history

face of each test sample and the evolution of the spot-wise whitening to the structural response of the tests. The test set-up therefore consists of a midget tensile module of the company Kammrath & Weiss GmbH, which was installed in a light microscope (Keyence Model VHX-600 Digital Microscope). Muth (2018) presented the geometry and manufacturing of the test samples as well as the testing procedure in great detail in his work. Nevertheless, it should be mentioned at this point that, on the one hand, a special cutting die was produced in order to be able to produce miniature tensile specimens at all. The shape was chosen according to the available space within the miniature tensile testing machine. Basically, however, it can be said that the miniaturized test sample is only a scaling of the dog-bone tensile test specimen developed by Becker (2009). On the other hand, the base material was placed in a climatic chamber at 140 °C and pressurized to obtain the typical material properties of TSSA. This procedure is the same as that proposed by Sitte et al. (2011).

The cyclic uniaxial tensile tests were performed in standard climate with a constant displacement rate of $v_{\mathrm{CUT}} = 3.75$ mm/min, which is the fastest displacement rate of the tensile module. The force was measured with a 5000 N load cell. The specimen was clamped using a mechanical screw-clamping system, so that a slight slipping out of the specimen could be detected during testing. Since a local measurement of Hencky strains using digital image correlation was not possible, the results of five test samples are shown in Fig. 8 in the form of global force-displacement curves. Additionally, the load history is presented for reasons of clarity.

The results show the Mullins effect clearly, in which a pronounced softening of the material can be seen for the unloading paths. Looking at the reloading paths, they follow the unloading paths up to the maximum stretch applied so far. Exceeding this point, the so-called virgin path is followed again, which corresponds to the material response of a non-cyclic loaded uniaxial tensile test. The material behavior to be seen corresponds to the classical definition of the Mullins effect (Diani et al. 2009) without exhibiting healing effects. Furthermore, it is noticeable that the structural responses scatter strongly, especially at small deformations, which is due to the slipping out of the specimens due to the mechanical clamping. Nevertheless, the structural responses show a typical behavior under cyclic loading. Finally, it should be mentioned that the effect of whitening, especially in the virgin loading paths, could also be clearly seen in the cyclical experiments. During the unloading and reloading paths, the described whitening remains at approximately the same level until one again loads beyond the point of maximum achieved elongation.

B Cyclic pancake tests

In order to experimentally investigate TSSA under an almost triaxial deformation condition, classical cyclic pancake tests were carried out according to the tests of Gent and Lindley (1959), in which two steel cylinders were glued with TSSA and then axially pulled. The pancake test samples were tested with a diameter of $d_0 = 50.0$ mm. The pancake test specimens were produced in an autoclave according to the specifications of Sitte et al. (2011). In the test series of the classical pancake tests, seven specimens with a diameter of $d_0 = 50.0$ mm were tested in a standard climate under cyclic axial loading. The local deformations of

the adhesive were recorded utilizing the DIC. For this purpose, the specimen was first coated with a white primer in the area of the measuring field and then a black speckle pattern was applied to carry out the local strain measurement. In contrast to the cyclic uniaxial tensile tests (see "Appendix A"), the pancake tests show only slight deformations, so that a higher resolution of the occurring deformations is necessary. This is also the reason why the speckle pattern for these tests could be applied by spraying. Generally, the cyclic pancake tests were performed to explain whether the cavitation effect is reversible and to study the Mullins effect in heavily constrained tensile tests. To characterize the material softening due to the Mullins effect, it is necessary to approach defined load levels with the testing machine and then unload it to a zero force level again. Since it was not possible to use the local displacement signal of the adhesive joint, which was measured optically, as a control signal for the testing machine, the cyclic pancake tests were performed force-controlled. This was necessary because although the global displacement of the traverse of the testing machine could be regulated to zero, compressive stresses could occur in the material due to slightly viscous effects or a permanent set of strains of the polymer. In order to make the axially displacement-controlled and cyclically force-controlled pancake tests comparable, the force-rate was set to $v_{\mathrm{CPC}} = 9.0$ N/s, which corresponds approximately to the displacement-rate used by Drass et al. (2018a). Preliminary investigations showed no differences in the structural response of displacement- or force-controlled experimental tests. Accordingly, the proposed variant of the test procedure is legitimate. It should also be noted that all tests were carried out at room temperature to ensure comparability with the non-cyclical experimental studies described above.

Seven cyclic pancake tests were tested in a standard climate. All test specimens were manufactured in an autoclave. The test set-up and the test samples are similar to the PC-I test series according to Drass et al. (2018a), in which two stainless steel point holders were glued with TSSA and pulled axially. The first load cycle ended after reaching a force of 6000 N and was then unloaded to a zero force level. With each load cycle, the load level was increased by 1000 N until the material was completely damaged. For reasons of comparability, the cyclic heavily constraint pancake tests were also performed at room temperature.

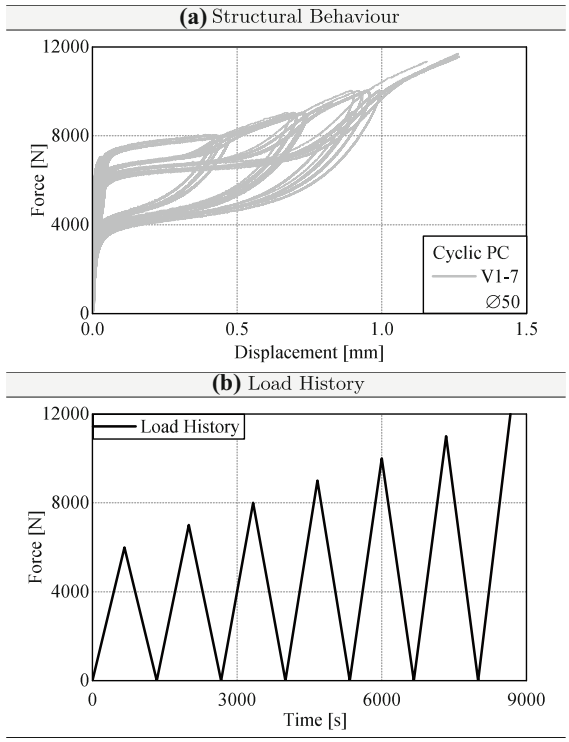

Fig. 9 Experimental results of cyclic pancake tests for TSSA **a** force versus local displacement; **b** load history

The structural behaviour of the cyclic pancake tests is shown in Fig. 9. In addition, the load history is presented for reasons of clarity. The cyclic pancake tests performed show a very complex structural behaviour, which can be divided into three essential parts. The first part of the structural response describes the loading path, also called the virgin path. It corresponds to the load path of the conventional pancake tests under uniaxial load and has the highest structural response to be achieved. The bifurcation load is approximately 7000 N. The second part describes the unloading path, which exhibits a substantially reduced stiffness compared to the virgin loading path. A very unusual behaviour occurs during reloading, which describes the third part of the classification of the structural response of cyclic pancake tests. In contrast to the Mullins effect, the unloading and reloading paths are not identical. It is clearly visible that a recovery or healing effect occurs during the reloading process, whereby the reloading curve is clearly above the unloading curve and below the virgin loading curve. This implies that, in contrast to the classical Mullins effect, the majority of the mechan-

ical hysteresis is not caused by effects like bond breakage of polymer chains or filler rupture, but rather the growth and shrinkage of voids in the material under hydrostatic load. The effects associated with the classical Mullins effect are, for some materials and to a specific amount, reversible, but only under thermal treatment. However, some amount of the softening seems to be permanent. This could be caused by the classical Mullins effect due to deviatoric deformations inside the pancake test, which especially occurs at the outer area of the sample. It is worth mentioning that all unloading paths converge to a force level of about 3600 N at almost zero axial deformation.

Looking at the structural behavior, it can be assumed that the recovery or healing effect is due to elastic pore growth and shrinkage, which in combination with the Mullins effect and possible bond breakage and filler rupture leads to the present result. The cavitation effect must be reversible so that the reloading curve is above the unloading curve. However, since the reloading path remains below the virgin curves, an additional Mullins damage must occur. As it has already been shown in the cyclic uniaxial tensile tests, no remarkable hysteresis develops during testing. Hence, the phenomena mentioned must occur particularly in triaxially stressed areas, which are all but the peripheral areas in the pancake test sample. The hypothesis of elastic void growth in the loading paths (virgin loading and reloading) can be further consolidated, since the initial stiffness always corresponds to the virgin stiffness even after several load cycles. Furthermore, it should be noted that healing starts abruptly without the use of temperature storage or the use of relaxation by incorporating holding times in the test sequence. Interestingly, all reloading curves result in a uniform force level of 6000 N, which, however, is below the virgin bifurcation load. However, following the reloading path and reaching the previously reached maximum elongation corresponding to the virgin curve, both curves are again identical.

C Material parameters-extended pseudo-elastic cavitation model

Summary of the material parameters for TSSA for the presented extended pseudo-elastic cavitation model from Sect. 3.

Table 2 Optimised material parameters for TSSA for extended pseudo-elastic cavitation model

Material model	Parameters
Isochoric Neo-Hooke model	$\mu = 2.6652$
Pseudo-elastic cavitation model	$\kappa_0 = 0.0004$
	$\kappa_1 = 0.2699$
	$\kappa_2 = 0.2501$
	$\kappa_3 = -0.195$
Isochoric Mullins effect	$r = 0.5882$
	$m = 2.0$
Volumetric Mullins effect	$r_{\text{vol}} = 0.45$
	$m_{\text{vol}} = 0.2$
Volumetric healing effect	$r_{\text{heal}} = 0.67$
	$m_{\text{heal}} = 0.07$

References

Bartels, N.: Experimental and numerical investigation considering cyclic, volumetric damage of structural silicones. Master thesis, Technische Universität Darmstadt (2018)

Becker, F.: Entwicklung einer beschreibungsmethodik für das mechanische verhalten unverstärkter thermoplaste bei hohen deformationsgeschwindigkeiten. Doctoral thesis, Martin-Luther-Universität Halle-Wittenberg (2009)

Blanchard, A.F., Parkinson, D.: Breakage of carbon-rubber networks by applied stress. Ind. Eng. Chem. **44**(4), 799–812 (1952). https://doi.org/10.1021/ie50508a034

Bouasse, H., Carrière, Z.: Sur les courbes de traction du caoutchouc vulcanisé. Ann. Fac. des Sci. Toulouse Math. 2e série **5**(3), 257–283 (1903)

Bueche, F.: Molecular basis for the Mullins effect. J. Appl. Polym. Sci. **4**(10), 107–114 (1960). https://doi.org/10.1002/app.1960.070041017

DAmbrosio, P., De Tommasi, D., Ferri, D., Puglisi, G.: A phenomenological model for healing and hysteresis in rubber-like materials. Int. J. Eng. Sci. **46**(4), 293–305 (2008)

Diani, J., Fayolle, B., Gilormini, P.: A review on the Mullins effect. Eur. Polym. J. **45**(3), 601–612 (2009). https://doi.org/10.1016/j.eurpolymj.2008.11.017

Drass, M., Schneider, J., Kolling, S.: Damage effects of adhesives in modern glass façades: a micro-mechanically motivated volumetric damage model for poro-hyperelastic materials. Int. J. Mech. Mater. Des. (2017). https://doi.org/10.1007/s10999-017-9392-3

Drass, M., Schneider, J., Kolling, S.: Novel volumetric helmholtz free energy function accounting for isotropic cavitation at finite strains. Mater. Des. **138**, 71–89 (2018a). https://doi.org/10.1016/j.matdes.2017.10.059

Drass, M., Schwind, G., Schneider, J., Kolling, S.: Adhesive connections in glass structures–part I: experiments and analytics on thin structural silicone. Glass Struct. Eng. **3**(1), 39–54 (2018b). https://doi.org/10.1007/s40940-017-0046-5

Drass, M., Schwind, G., Schneider, J., Kolling, S.: Adhesive connections in glass structures–part II: material parameter identification on thin structural silicone. Glass Struct. Eng. **3**(1), 55–74 (2018c). https://doi.org/10.1007/s40940-017-0048-3

Drass, M., Du Bois, P., Schneider, J., Kolling, S.: Pseudo-elastic cavitation model–part I: finite element analyses on thin silicone adhesives in façades. Glass Struct. Eng. (2019) (Forthcoming)

Flory, P.J.: Thermodynamic relations for high elastic materials. Trans. Faraday Soc. **57**, 829–838 (1961). https://doi.org/10.1039/TF9615700829

Gent, A.N., Lindley, P.B.: Internal rupture of bonded rubber cylinders in tension. Proc. R. Soc. Lond. A Math. Phys. Eng. Sci. **249**(1257), 195–205 (1959). https://doi.org/10.1098/rspa.1959.0016

Hanson, D.E., Hawley, M., Houlton, R., Chitanvis, K., Rae, P., Orler, E.B., Wrobleski, D.A.: Stress softening experiments in silica-filled polydimethylsiloxane provide insight into a mechanism for the Mullins effect. Polymer **46**(24), 10989–10995 (2005). https://doi.org/10.1016/j.polymer.2005.09.039

Houwink, R.: Slipping of molecules during the deformation of reinforced rubber. Rubber Chem. Technol. **29**(3), 888–893 (1956). https://doi.org/10.5254/1.3542602

Kraus, G., Childers, C.W., Rollmann, K.W.: Stress softening in carbon black-reinforced vulcanizates. Strain rate and temperature effects. J. Appl. Polym. Sci. **10**(2), 229–244 (1966). https://doi.org/10.1002/app.1966.070100205

Lazopoulos, K.A., Ogden, R.: Nonlinear elasticity theory with discontinuous internal variables. Math. Mech. Solids **3**(1), 29–51 (1998). https://doi.org/10.1177/108128659800300103

Mullins, L.: Effect of stretching on the properties of rubber. Rubber Chem. Technol. **21**(2), 281–300 (1948). https://doi.org/10.5254/1.3546914

Mullins, L.: Permanent set in vulcanized rubber. Rubber Chem. Technol. **22**(4), 1036–1044 (1949). https://doi.org/10.5254/1.3543010

Mullins, L., Tobin, N.R.: Stress softening in rubber vulcanizates. part I. Use of a strain amplification factor to describe the elastic behavior of filler-reinforced vulcanized rubber. J. Appl. Polym. Sci. **9**(9), 2993–3009 (1965). https://doi.org/10.1002/app.1965.070090906

Muth, J.: Development of hypotheses concerning the stress-whitening effect in structural silicones based on midget-tension tests. Bachelor thesis, Technische Universität Darmstadt (2018)

Ogden, R., Roxburgh, D.G.: A pseudo-elastic model for the mullins effect in filled rubber. Proc. R. Soc. Lond. Ser. A Math. Phys. Eng. Sci. **455**(1988), 2861–2877 (1999). https://doi.org/10.1098/rspa.1999.0431

Sitte, S., Brasseur, M., Carbary, L., Wolf, A.: Preliminary evaluation of the mechanical properties and durability of transparent structural silicone adhesive (TSSA) for point fixing in glazing. J. ASTM Int. **10**(8), 1–27 (2011). https://doi.org/10.1520/JAI104084

Zhang, X., Andrieux, F., Sun, D.: Pseudo-elastic description of polymeric foams at finite deformation with stress softening and residual strain effects. Mater. Des. **32**(2), 877–884 (2011). https://doi.org/10.1016/j.matdes.2010.07.004